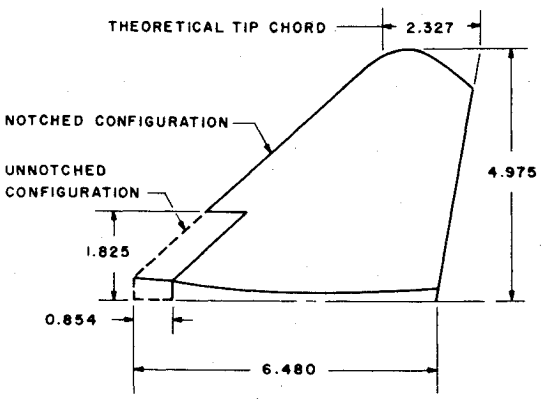

Fig. 4 Horizontal stabilizer plan form. All dimensions are in inches. Note: Unnotched stabilizer has approximately 5.4% more area.

motions: one flight and two wind tunnel generated. The longitudinal maneuver, Fig. 2, was generated from a horizontal stabilizer (δh) doublet at a trimmed flight condition. The lateral/directional maneuver, Fig. 3, represents an aileron doublet obtained by differentially deflecting the model horizontal stabilizers (δD). The differential deflections occur at about a nominal horizontal stabilizer setting (δh) of -15.8 deg. The flight data were acquired with an "unnotched" horizontal stabilizer configuration, Fig. 4. Flight test, with both "notched" and "unnotched" horizontal stabilizers, showed no measurable change in aircraft trim angle of attack (α) with either stabilizer. Because of this, the initial wind tunnel simulated motion was acquired with the 1/20-scale model utilizing an existing "notched" horizontal stabilizer. As seen in both the longitudinal and lateral/directional motion [pitch (q), yaw (r), roll (p), angle of sideslip (β)], the wind tunnel maneuvers with the "notched" stabilizer have motion frequencies near the flight data but show large deficiencies in amplitude. Also the angle of attack at which the wind tunnel model is trimmed for the lateral oscillations of Fig. 3 is approximately 4 to 6 deg lower than the RPV model for the nominal δh setting of -15.8 deg. The assumption that the "notched" stabilizer would have nearly equal the effectiveness of the "unnotched" version in the wind tunnel as seen in flight was a poor one.

An "unnotched" horizontal stabilizer was incorporated on the wind tunnel model and new longitudinal and lateral/directional maneuvers were generated, Figs. 2 and 3, respectively. The amplitude discrepancies between RPV and captive motion have decreased, and generally good data correlation exist in all motion planes.

The remaining deficiency in amplitude continued to be the result of a less effective horizontal stabilizer on the wind tunnel model. To achieve exact agreement between captive motion generated in the wind tunnel and flight motion, a better aerodynamic representation of the flight vehicle than was provided by the wind tunnel model must exist.

Conclusions

Captive testing provides a means of conducting an aircraft motion analysis study without the acquisition of static aerodynamic data matrices. An aircraft model with a full compliment of aerodynamic control surfaces is required for generating complex aircraft maneuvers although aircraft dynamic stability characteristics may be investigated without control movements.

References

[1] Partridge, D.W. and Pecover, B.E. "An Application of the R.A.E. Wind-Tunnel/Flight Dynamics Simulator to the Low-Speed Dynamics of a Slender Delta Aircraft (HP 115)," Royal Aircraft Establishment, Farnborough, England, R & M No. 3669, 1971.

[2] Butler, R.W. "Evaluation of a Wind Tunnel Technique to Determine Aircraft Departure Characteristics," Arnold Engineering Development Center, Arnold AFB, Tenn., AEDC-TR-73-183, 1973.

[3] Nichols, J. H. "A Method for Computing Trajectories of Stores Launched from Aircraft," David Taylor Model Basin, Bethesda, Md., R.P. 1978,1964.

Potential Flow about Impulsively Started Rotors

J. Michael Summa*
The University of Texas at Austin, Austin, Texas

Nomenclature

B	= number of blades
B_i	= normal velocity components of the blade at element i
C_T	= thrust coefficient
NC,NS	= element number along chord and span
R	= rotor radius
V	= axial velocity
Γ	= circulation
$\Delta\phi_p^w$	= potential jump across wake element p
θ	= pitch angle
λ	= advance ratio, $\lambda = V/\Omega R$
σ_j	= doublet strength per unit area of element j
ψ	= azimuth angle
Ω	= rotational speed

Introduction

In Ref. 1 a method was developed for the calculation of unsteady three-dimensional lifting potential flows and was applied to impulsive motion of wings and rotors. This work was motivated by the difficulties encountered by previous methods for predicting static thrust on propellers and rotors,[2] as well as by inadequacies in representing the complicated wake geometries observed behind highly loaded wings and in the vicinity of multi-bladed propellers or rotors with low inflow velocity. Here, some of the results for the rotor problem are illustrated.

Formulation

By using Green's theorem,[3] an exact integral solution for the inviscid incompressible flowfield due to rotor motion is obtained, wherein by a continuous distribution of doublets on each of the blades and their respective wakes. For the case of a rotor in combined rotational and axial motion, application of the exact surface tangency condition and evaluation of the resulting surface integrals by means of a discrete set of small surface elements yield the following matrix equation that is to be solved

$$[A_{i,j}]\ \{\sigma_j\} = \{B_i\} - [A^w_{i,p}]\ \{\Delta\phi^w_p\} \qquad (1)$$

Here, $A_{i,j}$ is the normal induced velocity coefficient on the ith element of blade 1 due to the doublet distribution of the jth element of each blade. $A^w_{i,p}$ is similarly defined. The numerical solution is obtained in a step-by-step fashion, rotors being impulsively started from rest. Quadrilater sur-

Presented as Paper 75-126 at the AIAA 13th Aerospace Sciences Meeting, Pasadena, Calif., Jan. 20-22, 1975; submitted Feb. 24, 1975; revision received Feb. 6, 1976. This work was sponsored by the Air Force Office of Scientific Research under Contract F44620-72-C-0026.

Index categories: Rotary Wing Aerodynamics; Nonsteady Aerodynamics.

*Assistant Professor, Department of Aerospace Engineering and Engineering Mechanics. Member AIAA.

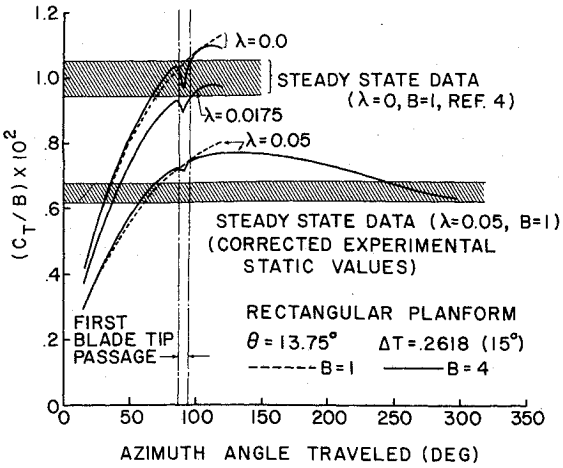

Fig. 1 Indicial thrust per blade for rotors started impulsively.

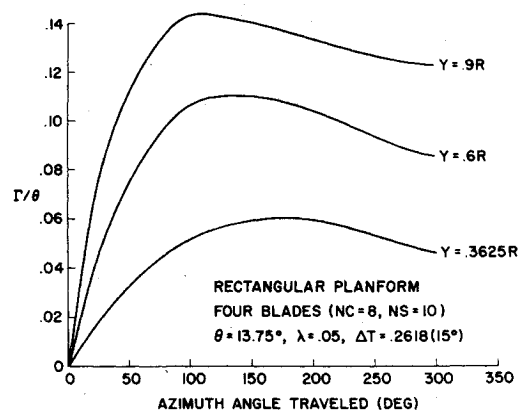

Fig. 2 History of instantaneous circulation.

face elements with "step" doublet distributions are employed. The geometry and vorticity distribution of the wakes, including "curling up" of the rear and side edges, are generated for each time step via the Kutta-Joukowski condition at trailing edges and the dynamic and geometric free surface conditions on all wake surfaces. Consequently, this technique allows for the generation of free-wake geometries, the coupling of the deformed wake with blade loading, and near wake interference in addition to accounting for exact blade surface shape.

Calculations

Numerical calculations were performed for a single- and four-bladed rotor of simple geometry (rectangular planform, no twist) with and without thickness.[1] Because of limited computer funds, only a minimum number of blade elements required to verify the method was used in each case, and a time step equivalent to a change in azimuth angle of 15° was employed. Results are illustrated for the zero thickness cases.

The calculated instantaneous thrust coefficient per blade for the single-bladed rotor planform and the four-bladed version is shown in Fig. 1. Numerical results for three different advance ratios are presented. Single-bladed data was calculated for 120° of azimuth travel while one case for the four-bladed configuration was allowed to run for 300° of azimuth travel. The outstanding feature of these calculations is that the indicial thrust coefficient initially overshoots and then approaches asymptotically from above its final steady-state value. This property is attributable to the presence of the vortex wake system. Basically, the loading per blade is increased as the blade approaches the upwash created by the starting vortex shed by the fore-running blade (Fig.1, to $\psi \sim 90°$). As the blade passes above the starting vortex, the induced effects on the blade undergo roughly a step function change in the opposite direction, i.e., a downwash, and the thrust decreases as shown in Fig. 1. The influence of the starting vortex is of course diminished with increasing advance ratio – i.e., axial distance from the blade. Additionally, the instantaneous circulation (Fig. 2) does not exhibit a "spike decrement" paralleling that of the thrust per blade. Thus, the thrust loss comes about *primarily* through the apparent mass term. The effect on the circulation by the step change due to the starting vortex requires a finite duration of time to make itself felt. Meanwhile, the blade moves past the starting vortex, its influence wanes, and the loading partially recovers. At later times, the close proximity of the unsteady rolled-up tip vortex to the blade dominates the induced velocities associated with the wake and creates a downwash throughout the blade span, except very near the tip. Consequently, the growth of airloads and circulation due to indicial motion is eventually exceeded by the decrement caused by the wake system. Therefore, the thrust as well as the instantaneous circulation reach a maximum and then decay toward a steady-state value as shown in Figs. 1 and 2.

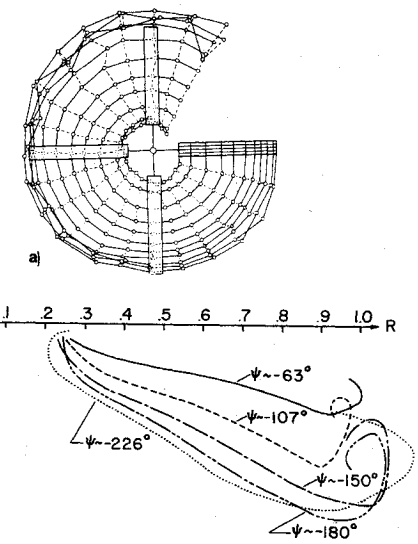

Fig. 3 Wake geometry for an impulsively started rotor: a) top view; b) constant azimuthal sections.

For very small advance ratios, the root vortex passed through the following blade due to the large time step size and local roll-up. To avoid this problem, $\lambda = 0.05$ was chosen for the lengthly calculation. The experimental thrust coefficient[4] in hover was corrected by simple momentum theory for this advance ratio. Although the final calculated C_T/B is within the corrected experimental accuracy band, a steady state has not yet been achieved and C_T/B should eventually reach a lower value. In addition, some irregularities developed in the wake at the tip after one half of a revolution. Consequently, conclusions about accurate convergence to a final steady state would be inappropriate, even through the influence of the wake irregularity on the thrust was evidently small.

The wake geometry for the four-bladed rotor at an advance ratio of 0.05 after 300° of azimuthal travel is shown in Fig. 3a (as seen from above the rotor) and 3b (constant azimuthal sections). Only the primary blade wake is shown. Initial tip vortex roll-up and contraction by the time of the first blade passage were properly modeled. Also encouraging was the grouping of the trailing vortex filaments into a strong rolled-up tip vortex and a weaker vortex sheet for the inboard portion of the wake. However, an irregularity developed in the tip vortex location due to the presence of wake surfaces from other blades. This behavior evidently occurs when a wake control point in the tip region falls close to another element, and unrealistically large distortions are predicted due to the large time step size used. Remedies for this problem such as

finite core size and use of artificial viscosity are currently being investigated.

Conclusions

A surface singularity method has been developed for the "exact" calculation of unsteady three-dimensional lifting potential flows including the effects of wake roll-up. Numerical calculations of the early stages of the flowfield for a rotor impulsively started revealed that the indicial thrust and circulation overshoot shortly after motion starts and then approach asymptotically from above their steady-state values. Additionally, the modeling of the distorted rotor wake geometry was partially successful with initial tip roll-up and contraction being present. However, more work is required before an accurate description of the complete wake geometry can be obtained.

References

[1]Summa, J. M., "Potential Flow About Three-Dimensional Streamlined Lifting Configurations with Application to Wings and Rotors," Stanford University, Stanford, Calif., SUDAAR 485, Sept. 1974.

[2]Cheney Jr., M. C. and Landgrebe, A. J., "Rotor Wakes – Key to Performance Prediction," AGARD – CPP-111, AGARD Conference on Aerodynamics of Rotor Wings, Marseilles, France, Sept. 1972.

[3]Lamb, S. H., *Hydrodynamics*, 6th ed., Dover Publications, New York, 1932, pp. 57-61.

[4]Gray, R. B. and Brown, G. W., "A Vortex-Wake Analysis of a Single-Bladed Hovering Rotor and a Comparison with Experimental Data," AGARD-CPP-111, AGARD Conference on Aerodynamics of Rotory Wings, Marseille, France, Sept. 1972.

Inlets for High Angles of Attack

Brent A. Miller*
NASA Lewis Research Center, Cleveland, Ohio

Nomenclature

A_e = flow area at diffuser exit
A_t = flow area at throat (minimum area)
$\mathfrak{D}_{max}$ = inlet total pressure distortion [(maximum total pressure)-(minimum total pressure)] / (average total pressure)
M_e = Mach number at diffuser exit
p = surface static pressure
P_0 = freestream total pressure
V_0 = freestream velocity
x = axial distance from highlight
α_{sep} = angle of attack (measured between freestream velocity and inlet centerline) resulting in inlet flow separation, deg.

Introduction

INLETS capable of operating successfully to high angles of attack are required for STOL and some VTOL aircraft concepts. In the STOL application, high angles of attack result from the large upwash generated by high wing lift coefficients.[1] With VTOL aircraft, large angles of attack may be generated during the transition maneuver. Analytical and experimental studies[2-6] indicate that increasing lip thickness, or contraction ratio, can substantially improve the ability of the inlet to tolerate large flow angles. However, this approach generally results in inlet lip designs that are in conflict with the lip shape desired for most efficient cruise operation. In this

Received Dec. 12, 1975; revision received Jan. 19, 1976.
Index category: Aircraft Aerodyanmics (including Component Aerodynamics).
*Research Engineer.

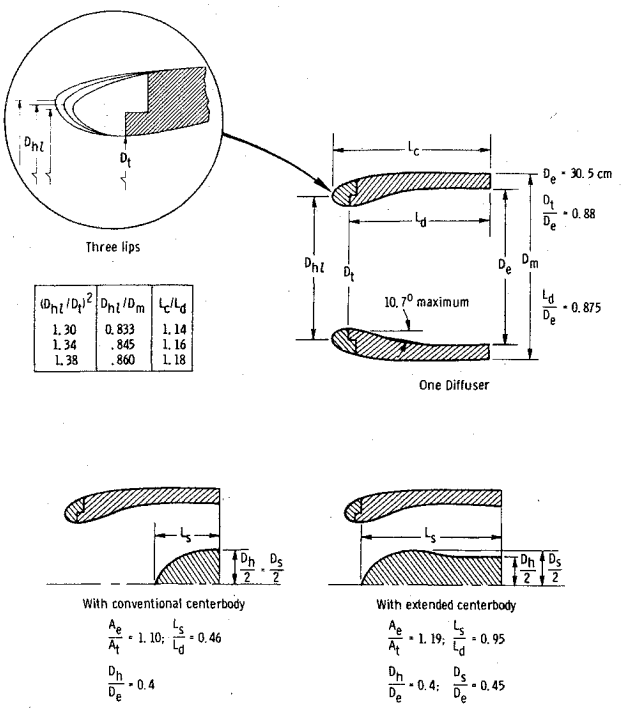

Fig. 1 Inlet geometry and nomenclature.

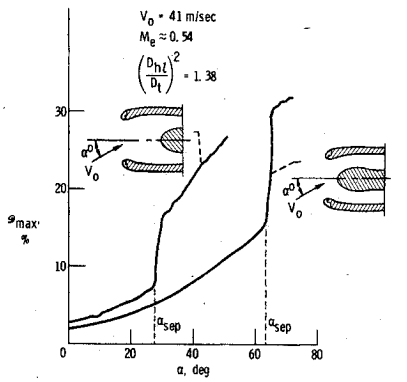

Fig. 2 Increase in distortion with increasing angle of attack and flow separation.

Note the results of low-speed wind tunnel tests are presented that suggest another approach in designing for high angles of attack.

Apparatus and Results

An inlet design for high-speed subsonic flight was tested in the Lewis Research Center's 2.75 by 4.58 meter (9×15 ft) V/STOL wind tunnel at a forward velocity of 41 meters per sec (80 knots). This velocity is representative of STOL takeoff and landing conditions and VTOL transition.

The geometry and nomenclature used to describe the inlet lips and diffuser tested are shown in the top sketch of Fig. 1. Three removable entry lips, having contraction ratios, $(D_{hl}/D_t)^2$, of 1.30, 1.34, and 1.38 were tested with a single diffuser. The internal contour of each entry lip was an ellipse with a major to minor axis ratio of 2.0. The NACA-1 cowl shape was used for the entry lip external forebody. As indicated by the table of Fig. 1, the ratio of inlet cowl length to diffuser length, L_c/L_d, increased slightly with increasing lip contraction ratio. This was due to the increase in internal lip axial length that resulted from maintaining a constant major to minor axis ratio.

Each lip and diffuser assembly was tested to determine its tolerance to angle of attack, with first a conventional cen-